

Multispectral photoacoustic imaging of nerves with a clinical ultrasound system

Jean Martial Mari*^a, Simeon West^b, Paul C. Beard^a, Adrien E. Desjardins^a

^aDepartment of Medical Physics and Bioengineering, University College London, London, United Kingdom; ^bUniversity College Hospital, London, United Kingdom

ABSTRACT

Accurate and efficient identification of nerves is of great importance during many ultrasound-guided clinical procedures, including nerve blocks and prostate biopsies. It can be challenging to visualise nerves with conventional ultrasound imaging, however. One of the challenges is that nerves can have very similar appearances to nearby structures such as tendons. Several recent studies have highlighted the potential of near-infrared optical spectroscopy for differentiating nerves and adjacent tissues, as this modality can be sensitive to optical absorption of lipids that are present in intra- and extra-neural adipose tissue and in the myelin sheaths. These studies were limited to point measurements, however. In this pilot study, a custom photoacoustic system with a clinical ultrasound imaging probe was used to acquire multi-spectral photoacoustic images of nerves and tendons from swine *ex vivo*, across the wavelength range of 1100 to 1300 nm. Photoacoustic images were processed and overlaid in colour onto co-registered conventional ultrasound images that were acquired with the same imaging probe. A pronounced optical absorption peak centred at 1210 nm was observed in the photoacoustic signals obtained from nerves, and it was absent in those obtained from tendons. This absorption peak, which is consistent with the presence of lipids, provides a novel image contrast mechanism to significantly enhance the visualization of nerves. In particular, image contrast for nerves was up to 5.5 times greater with photoacoustic imaging (0.82 ± 0.15) than with conventional ultrasound imaging (0.148 ± 0.002), with a maximum contrast of 0.95 ± 0.02 obtained in photoacoustic mode. This pilot study demonstrates the potential of photoacoustic imaging to improve clinical outcomes in ultrasound-guided interventions in regional anaesthesia and interventional oncology.

Keywords: Photoacoustic imaging, multi-spectral, spectroscopy, lipid, nerves, tendons.

1. INTRODUCTION

B-mode ultrasound imaging is widely used to guide minimally invasive procedures [1][2][3][4][5][6]. In these procedures, accurate identification of procedural targets is of primary importance to maximise successful outcomes and to minimise risks [7]. Misinterpretation of a patient's anatomy can lead to a wide range of complications. For instance, with nerve blocks, in which anaesthesia is injected in the region surrounding a nerve, these complications include intra-neural and intra-vascular injections [8][9]; with prostate biopsies, in which tissue is obtained for histological analysis, they include nerve damage [10].

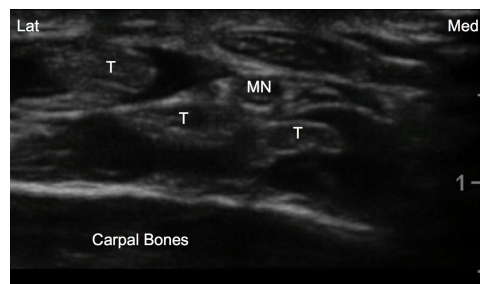


Figure 1. Conventional ultrasound B-mode scan of the hand in which tendons (T) and the median nerve (MN) are visible. The texture and intensity of the image renders the distinction between nerves and tendons difficult; this is underlined by the variability of the signal generated by tendons, which can vary significantly in their sonographic appearances.

* jm.mari@ucl.ac.uk; phone +44 020 7679 0200; fax 44 (0)20 7679 0255

During minimally invasive procedures, B-mode ultrasound imaging [11][12] is useful to visualise devices such as needles and to identify anatomical features [6]. However, in many situations, it can be challenging to identify nerves with high specificity. In particular, during ultrasound-guided nerve blocks, neural structures can have similar appearances to muscle, fascia, blood vessels and tendons. For instance, in differentiating nerves from tendons, despite having very different cellular architectures and molecular compositions, nerves can have very similar ultrasonic appearances to tendons in terms of their echogenicity and texture (Figure 1). Practitioners often use nerve stimulators to additionally identify nerves from similar looking structures [13], but these have a low sensitivity for intraneural placement and as such are no longer used by many. There is a clinical need to develop new techniques that can address this limitation of B-mode ultrasound imaging.

Photoacoustic (PA) imaging is a new modality that provides information about the molecular composition of tissues [14][15][16][18]. It is complementary to ultrasound imaging [19][20], in the sense that image formation relies upon the detection of acoustic signals but the transduction mechanism is fundamentally different. With ultrasound imaging, ultrasound waves are provided by the imaging probe and their reflections are detected [7][12]. With PA imaging, pulsed (nanosecond-scale) excitation light is provided to tissue and the ultrasound waves that are generated from absorption are detected [16]. Whereas contrast in ultrasound images derives from local differences in acoustic impedance [11], contrast in multispectral PA imaging derives from local variations in chromophore concentrations [18][21].

The potential for detecting nerves based on optical absorption from by lipids was successfully demonstrated using purely optical methods in previous studies [14][15], and the spectroscopic characteristics of lipids, as detected with PA, are well known [16][17]. However, to the authors' knowledge, the application of multispectral PA imaging to differentiate nerves from nearby tissue structures remains largely unexplored.

In this study, a custom multispectral PA system with a multi-element clinical ultrasound imaging probe was used to obtain a preliminary indication of the potential of PA imaging to differentiate nerves and tendons. Multispectral PA imaging involved the acquisition of a series of PA images that were generated with excitation light of different wavelengths. Imaging was performed on swine tissue *ex vivo*.

2. METHODS

Photoacoustic imaging was performed with an optical parametric oscillator (OPO) as the excitation light source (VersaScan L-532, GWU-Lasertechnik). This OPO was pumped by a frequency-doubled Q-switched Nd-YAG laser frequency with a wavelength of 532 nm, a repetition rate of 10 Hz, and a pulse width duration of 6 ns (Quanta-Ray INDI-40-10, Spectra-Physics). The idler beam of the OPO was coupled to a silica-silica optical fibre with a core diameter of 910 μm (FG910LEC, Thorlabs). The idler wavelengths were varied by motorised rotation of the nonlinear crystal in the OPO.

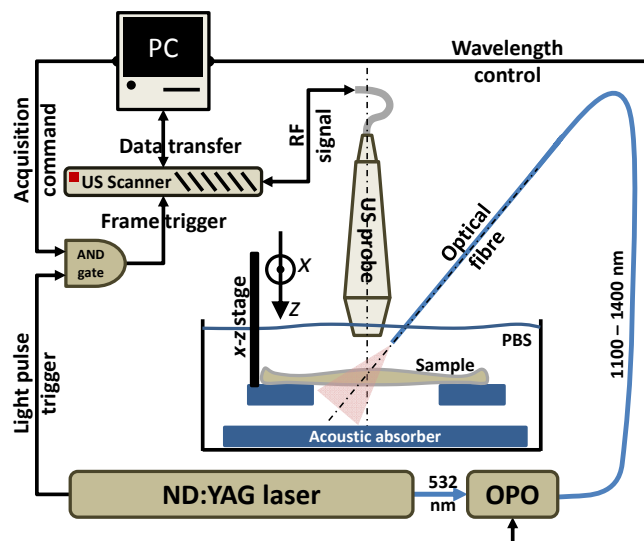


Figure 2. Schematic of the acquisition setup: ultrasound acquisitions were synchronised to the excitation light pulses, and controlled with a PC using an AND logic gate. The translation stages allowed for linear movement of the samples within the imaging region.

Images were acquired with a linear array of ultrasound transducer elements set within a clinical-style imaging probe, with dedicated hardware and a PC for data acquisition and beamforming (Ultravision, Winprobe, Florida, USA). The frequency range of the transducer elements, as rated by the manufacturer, was 5-14 MHz. The acquisition of photoacoustic images was triggered by the synchronisation signals of the OPO. An ultrasound B-mode image was acquired immediately after each photoacoustic image. An AND logic gate provided control over the rate at which images were acquired (Figure 2). The radio-frequency data from the transducer elements were sampled at 40 MHz and the computed envelopes of the corresponding time series were stored on a PC.

Nerves from the brachial plexus and tendons from the upper foot were excised from swine immediately post-mortem, maintained in phosphate buffered saline (PBS), and imaged within 24 hours. The swine were obtained from a different experiment that was unrelated to this study, at the Northwick Park Institute for Medical Research.

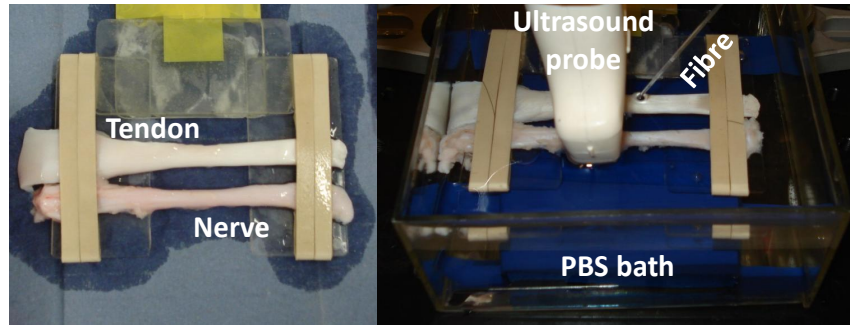


Figure 3. Tissue positioning during imaging: Left: Porcine nerve and tendon held in position; right: photoacoustic imaging configuration, with the light delivered through the optical fibre and the signal measured using a linear array ultrasound imaging probe.

The nerve and tendon were positioned at a depth of 1.5 cm from the ultrasound imaging probe with their axes perpendicular to the imaging plane (Figure 2) and imaged in phosphate buffered saline (PBS) solution. The experiment was conducted twice; the first time, the nerve and tendon were both maintained in the light cone exiting from the optical fibre; the second time, the nerve and tendon were held on a translation stage holder that allowed them to be moved relative to the optical fibre that provided illumination (Figure 3). The distance of the samples to the fibre was approximately 2 cm in the first case, 1 cm in the second, and the angle between the acoustical axis and the optical fibre was 30°. A first set of images was obtained with illumination centred on the nerve; subsequently, a second set of images was obtained with illumination centred on the tendon. In this way, the spatial position of the nerve in the first set of images was the same as that of the tendon in the second set. For each set of images, the idler wavelength was varied from 1100 nm to 1210 nm in steps of 5 nm. This wavelength range included the absorption peak of lipids at 1210 nm [15][16]. At each wavelength, 25 pairs of photoacoustic/ultrasound images were acquired.

To measure the spectroscopic variation of the photoacoustic signal, region of interests (ROIs) were manually drawn around the nerve and around the tendon in the first and second series of images, respectively. The two ROIs had identical dimensions. For each of the two ROIs, the mean and the standard deviation of the photoacoustic envelope data were calculated. To quantitatively compare the extent to which nerves and tendons could be differentiated with ultrasound and photoacoustic imaging, the image contrast was measured with the two ROIs.

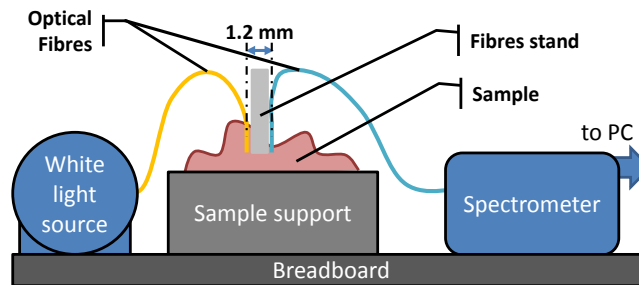


Figure 4. a) Optic fibres on their support for reflectance measurements; b) Reflectance measurement setup, using a broadband light source and a spectrometer connected to a PC.

The photoacoustic spectra and the B-mode wavelength-dependent amplitudes were acquired for the nerves and tendons, and the contrast [22] between them calculated from the mean spectrum amplitude in a 20 nm window centred at 1210 nm. Processing of photoacoustic and of ultrasound images was performed with custom scripts written in Matlab (Mathworks, Natick, NH, USA).

Following photoacoustic and ultrasound imaging, for a control experiment, optical reflectance spectroscopy was performed on the nerve and tendon samples. One silica-silica optical fibre with a core diameter of 105 μm (FG105LCA, Thorlabs) delivered broadband light to tissue from a Tungsten light source (HL2000, Ocean Optics, Florida, USA); a second received light scattered from tissue and delivered it to a spectrometer with an InGaAs array (NIRQuest 512, Ocean Optics, Florida, USA). The end faces of the two fibres were adjacent to tissue, with their centres separated by 1.2 mm. 30 spectra were acquired and averaged for the calculation. The spectrometer integration time was 60 ms.

Intensity-calibrated spectra $S(\lambda)$ were obtained with a white reflectance standard (SRS-99-010, Labsphere, New Hampshire, USA), using Equation (1):

$$S(\lambda) = \frac{S_L(\lambda) - S_B(\lambda)}{S_L^{Ref}(\lambda) - S_B^{Ref}(\lambda)} \quad (1)$$

In Equation (1), $S_L(\lambda)$ and $S_L^{Ref}(\lambda)$ are spectra measured from tissue and from the reflectance standard, respectively, and $S_B(\lambda)$ and $S_B^{Ref}(\lambda)$ are the corresponding background signals that were acquired with the light source shuttered.

3. RESULTS AND DISCUSSION

The nerve and the tendon have very similar appearances in Figure 5 with B-mode ultrasound imaging, as they did in Figure 1.

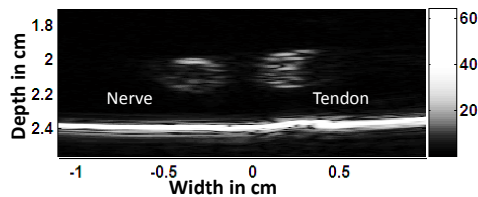


Figure 5. First experiment: Cross-sectional B-mode ultrasound images of a nerve (left) and a tendon (right) from the first experiment that were excised and placed in phosphate buffered saline.

In Figure 6-a and -b an example of overlay of PA frame and B-mode frame is provided. The grey level part of the image corresponds to the B-mode image, while the colour components are brought by the PA signal. Again from both images (especially Figure 6-b), it can be observed that the nerves and tendon are very similar based on the B-mode image only.

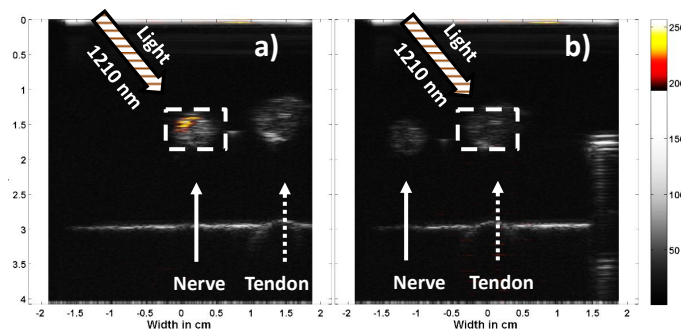


Figure 6. Second experiment: a) and b): Photoacoustic and B-mode overlaid images in water at 1210 nm, with the nerve and tendon successively brought in front of the light beam. The absorption of light at 1210 nm by the fat component of the nerve results in the apparition of the photoacoustic signature, absent in the tendon that has no fat. The mean amplitude of the photoacoustic signal is computed in the ROIs (dashed boxes) as function of light wavelength. The two ROIs are identical in both cases.

However, in Figure 6-a, the absorption of the 1210 nm light pulse by the fat enveloping the nerve give rise to a strong PA response from the part of the nerve exposed to light. When performed on the tendon, which has no fat the PA signal generated remains at the level of the noise.

The ROI used for mean PA signal amplitude calculation is provided in Figure 6, and the photoacoustic spectra obtained are displayed Figure 7. It can be observed in Figure 7-left that the PA signal issued from the tendon is largely independent from the light wavelength used. But the mean PA amplitude measured in the nerve is highly dependent on the wavelength, and forms a peak which reaches a maximum at 1210 nm, the absorption peak of lipids. This is further illustrated in Figure 7-right where the photoacoustic signal for the acquisitions at 1210 nm have been plotted.

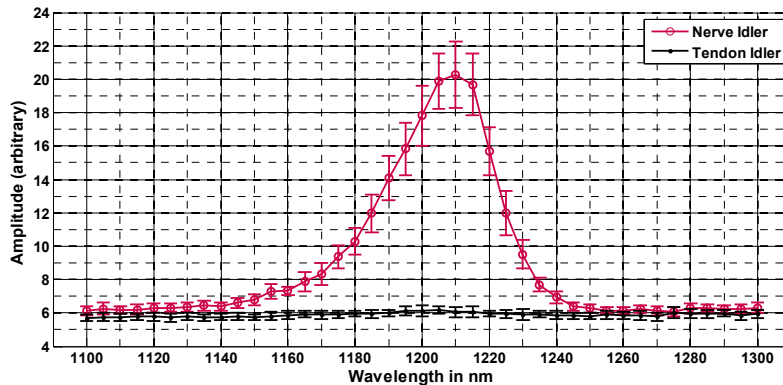


Figure 7. Second experiment: Photoacoustic spectra acquired on the Nerve and tendon between 1100 nm and 1300 nm every 5 nm. The 1210 nm peak is consistent with absorption of the light by the lipids present in the nerve, which is absent from the tendon.

For the first experiment, the photoacoustic image contrast between nerve and tendon was (0.82 ± 0.15) , which is 5.54 times greater than with conventional ultrasound imaging (0.148 ± 0.002) . For the second experiment the photoacoustic contrast was (0.95 ± 0.02) , which is 1.53 times greater than with conventional ultrasound imaging (0.619 ± 0.002) . The contrasts obtained in photoacoustic mode are very high, while the contrast in B-mode is variable, as mentioned earlier.

The reflectance results obtained for the spectroscopy experiments are presented in Figure 8. In both spectra, the low reflectance values in the 1400 – 1500 nm range are consistent with an absorption of the light by water. For the other part of the spectra, the shapes are similar, but for the 1150 – 1250 nm window, where the reflectance of the nerve drops. This demonstrates the presence of lipids in the nerve and illustrates its ability to absorb light in the right wavelength range.

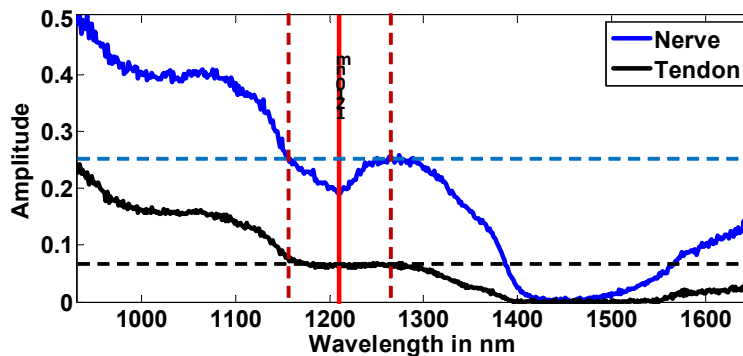


Figure 8. Control experiment: Optical reflectance spectra acquired from the surfaces of the nerve (blue) and tendon (black, dashed); the decreased signal around 1210 nm (around the red dash dotted vertical line, and between the two vertical red dashed lines) in the nerve spectrum, which is consistent with the presence of lipids, is absent in the tendon spectrum.

The different experiments performed confirm the presence of lipids in the imaged nerves, and demonstrate the ability to use the difference of lipid content to distinguish nerves from tendons using photoacoustics around the 1210 nm wavelength. While *in vivo* results on a larger number of cases are necessary, photoacoustic has potential as an imaging tool to distinguish nerves from tendons.

4. CONCLUSION

Multispectral photoacoustic imaging and conventional ultrasound imaging of nerves and tendons were performed with a clinical ultrasound imaging system. With an optical parametric oscillator as the pulsed excitation light source, photoacoustic images were acquired over the wavelength range of 1100-1300 nm, and photoacoustic spectra were obtained by averaging signal values in regions surrounding the tissue structures. In the images obtained from nerves, there were pronounced variations in the photoacoustic signals that were consistent with the presence of lipids; these features in the photoacoustic spectra were largely absent in multispectral images obtained from tendons. With an excitation light wavelength of 1210 nm, where optical absorption by lipids has a local maximum, the image contrast between nerves and tendons (0.82 ± 0.15) was 5.5-fold greater than it was with conventional ultrasound imaging (0.148 ± 0.002), with a maximum contrast of 0.95 ± 0.02 obtained in photoacoustic mode. Optical reflectance spectra, which were acquired with a broadband continuous-wave light source and a spectrometer, were consistent with the photoacoustic spectra in terms of the presence of features corresponding to optical absorption by lipids. We conclude that multispectral photoacoustic imaging has strong potential for improving nerve visibility during ultrasound-guided interventions.

REFERENCES

- [1] Narouze, S. N., [Atlas of Ultrasound-Guided Procedures in Interventional Pain Management 1st ed] Springer, New York (2010).
- [2] Eichenberger, U., Greher, M, Kirchmair, L., Curatolo, M., Moriggl, B., "Ultrasound-guided blocks of the ilioinguinal and iliohypogastric nerve: accuracy of a selective new technique confirmed by anatomical dissection" *Br J Anaesth.*, 97:238-243 (2006).
- [3] Hurdle, M. F, Weingarten, T. N., Crisostomo, R. A., Psimos, C., Smith, J., "Ultrasound-guided blockade of the lateral femoral cutaneous nerve: technical description and review of 10 cases" *Arch Phys Med Rehabil.*, 88:1362-1364 (2007).
- [4] Marhofer, P., Schrögenderfer, K., Wallner, T., Koinig, H., Mayer, N., Kapral, S., "Ultrasonographic guidance reduces the amount of local anesthetic for 3-in-1 blocks" *Reg Anesth Pain Med.*, 23:584-588 (1998).
- [5] Redborg, K. E, Sites, B. D., Chinn, C. D., et al., "Ultrasound improves the success rate of a sural nerve block at the ankle" *Reg Anesth Pain Med.*, 34:24-28 (2009).
- [6] Mari, J-M., Cachard, C., "Ultrasonic scanning of straight micro tools in soft biological tissues: methodology and implementation" *Ultrasonics*, 51(5):632-63 (2011).
- [7] Chan, V. W. S, Perlas A., McCartney, C. J. L., Brull, R., Xu, D. Q., Abbas, S., "Ultrasound guidance improves success rate of axillary brachial plexus block" *Can J Anaesth.*, 54:176-182 (2007).
- [8] Berg, A. P., Rosenquist R. W., "Complications of peripheral nerve blocks" *Techniques in Regional Anesthesia and Pain Management*, 11:133-140 (2007).
- [9] Bigeleisen, P. E., Moayeri N., and Groen G. J., "Extraneural versus intraneural stimulation thresholds during ultrasound-guided supraclavicular block" *Anesthesiology*, 110(6):1235-43 (2009).
- [10] Klein T.K., Palisaar R.G., Holz A., Brock, M., Noldusand J., Hinkel A., "The Impact of Prostate Biopsy and Periprostatic Nerve Block on Erectile and Voiding Function: A Prospective Study" *The journal of Urology.*, 184:1447-1452, (2010).
- [11] Mari, J-M., BouMatar, O., Blu, T., Cachard, C., Unser, M., "A bulk modulus dependent linear model for acoustical imaging" *J. Acoust. Soc. Am.*, 125:2413 (2009).
- [12] Mari, J-M., Cachard, C., "Acquire real time RF digital ultrasound data from a commercial scanner" *Technical Acoustics*, (2007).
- [13] Beach, M. L., Sites, B. D, Gallagher, J. D., "Use of a nerve stimulator does not improve the efficacy of ultrasound-guided supraclavicular nerve blocks" *J. Clin. Anesth.*, 18(8):580-4 (2006).
- [14] Balthasar, A., Desjardins, A. E., van der Voort, M., Roggeveen, S., Wang, K., Bierhoff, W., Kessels, A. G. H, Sommer, M., van Kleef, M., "Optical Detection of Vascular Penetration during Nerve Blocks: An in vivo Human Study" *Reg. Anesth. Pain Med.*, 37(3):277-82 (2012).
- [15] Brynolf, M., Sommer, M., Desjardins, A. E., van der Voort, M., Roggeveen S., Bierhoff W, Hendriks BHW, Rathmell J. P., Kessels, A. G. H., Söderman, M, Holmström, B., "Optical Detection of the Brachial Plexus for Peripheral Nerve Blocks: An in vivo Swine Study" *Reg Anesth Pain Med.*, 36:350–357 (2011).

- [16] Beard, P. C., "Biomedical photoacoustic imaging" *Interface Focus*, 1(4):602-631 (2011).
- [17] Allen, T. J., Hall, A., Dhillon, A. P., Owen, J. S., Beard, P. C. "Spectroscopic photoacoustic imaging of lipid-rich plaques in the human aorta in the 740 to 1400 nm wavelength range" *J. Biomed. Opt.*, 17(6):061209 (2012).
- [18] Cox, B., Laufer, J. G., Arridge, S. R., Beard, P. C. "Quantitative spectroscopic photoacoustic imaging: a review" *J. Biomed. Opt.* 17(6): 061202, (2012).
- [19] Cobbold, R., [Foundations of Biomedical ultrasound] Oxford University Press, (2007).
- [20] Atkinson, P., Woodcock, J.P. [Doppler Ultrasound and its use in clinical measurement]. Academic Press Inc. London (1982).
- [21] Laufer, J., Elwell, C. E., Delpy, D. T., and Beard, P. C., "In vitro measurements of absolute blood oxygen saturation using pulsed near-infrared photoacoustic spectroscopy: accuracy and resolution" *Physics in Medicine and Biology*, 50:4409-442 (2005).
- [22] Girard, M., Strouthidis, N., Ethier, R., Mari, J-M., "Shadow Removal and Contrast Enhancement in Optical Coherence Tomography Images of the Human Optic Nerve Head" *Invest. Ophthalmol and Vis. Sci.*, 52(10):7738-7748, (2011).